Title
CRITICAL RESOLVED SHEAR STRESS FOR A THERMAL DISLOCATION GLIDE THROUGH A RANDOM DISTRIBUTION OF POINT OBSTACLES

Author
Hanson, Kenton Lloyd.

Publication Date
1975-05-01

LBL-3924
c.1

CRITICAL RESOLVED SHEAR STRESS FOR ATHERMAL DISLOCATION GLIDE THROUGH A RANDOM DISTRIBUTION OF POINT OBSTACLES

Kenton Lloyd Hanson
(Ph. D. thesis)

May 1975

Prepared for the U. S. Energy Research and Development Administration under Contract W-7405-ENG-48

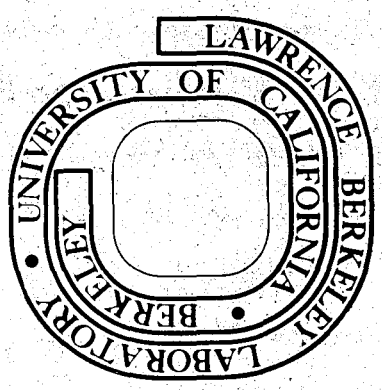

LBL-3924
c.1

DISCLAIMER

CRITICAL RESOLVED SHEAR STRESS FOR ATHERMAL DISLOCATION GLIDE THROUGH A RANDOM DISTRIBUTION OF POINT OBSTACLES

Table of Contents

CRITICAL RESOLVED SHEAR STRESS FOR ATHERMAL DISLOCATION GLIDE THROUGH A RANDOM DISTRIBUTION OF POINT OBSTACLES

Kenton Lloyd Hanson

Inorganic Materials Research Division, Lawrence Berkeley Laboratory and Department of Materials Science and Engineering, College of Engineering; University of California, Berkeley, California

ABSTRACT

The critical resolved shear stress for athermal dislocation glide through a random distribution of point like barriers is examined. An upper bound for the strength determining dislocation configuration is derived by employing the extinction theorem of stochastic branching process in probability theory. The solution yields the critical resolved shear stress, distribution of forces, and mean segment length. Also, a new general and efficient computer simulation for this problem is described. The results of the analytic solution are compared with the computer simulation and show good agreement. The analytic solution is then extended to the case of a random distribution of obstacles having an arbitrary distribution of strengths. The extended solution shows good agreement with computer simulation with respect to the critical resolved shear stress, distribution of forces, mean segment length, and concentration of obstacle types found on the strength determining configuration.

I. INTRODUCTION

A. General Problem Area

The achievement of a microstructure-based theory of the mechanical behavior of engineering alloys remains one of the central objectives of basic research in metallurgy. Its engineering importance is two-fold. First, a predictive theory of mechanical behavior is needed to provide a firm basis for materials selection and engineering design with real materials. Second, an interpretive theory of mechanical behavior is needed to guide metallurgical research in the design of new alloys to meet advanced engineering needs. The complexity of the mechanical behavior of real materials suggests that accurate, detailed theories will be slow in coming (as they have been). On the other hand, the evident potential engineering benefit to be derived from successful research would certainly seem to justify a sustained, systematic effort.

A typical problem in the mechanical behavior of engineering alloys sets up essentially as follows (modifying the concise discussion of Friedel[9]). An alloy consists of an aggregate of individual crystalline grains. Each of those is described by its composition, its crystal structure, its defect structure (including point defects, the network of existing dislocations, and the type and distribution of included voids or precipitates), its size and shape, and the nature of the grain boundaries which define its contact with adjacent grains. The state of stress within an individual grain depends on the applied load, the modification of that load by the geometry of the polycrystalline structure, and the state of internal stress within the body. The response to that stress depends on its magnitude and resolution on the various

potential slip planes within the grain. The response is initially elastic, with a small anelastic supplement due to the bowing or recoverable motion of dislocations, and to short range chemical arrangements. To initiate plastic deformation, dislocations must be created or liberated onto slip planes bearing a resolved shear stress of sufficient magnitude to sustain glide. To induce gross yielding of the polycrystalline alloy the resulting crystallographic slip must be accommodated at grain boundaries and propagated from grain to grain across the body. To sustain plastic deformation, the applied load must adjust to changes in the mechanical state of the body as deformation proceeds. The deformation process ultimately terminates in fracture or failure through plastic instability.

The sequence of processes listed above suggests several natural entry points for theoretical research. One of the most interesting and important[13] of these is the problem of yield and initial deformation in a grain or single crystal which is assumed to contain dislocations (or active sources of dislocations) together with microstructural features which act as barriers to free dislocation glide. The bulk of prior research (summarized in references 9 and 13) argues that this is a central problem in the deformation of engineering materials. Potentially mobile dislocations may generally be assumed to exist in a metal and the native lattice resistance to glide may generally be assumed small compared to that offered by such internal barriers as point defects, "forest" dislocations, precipitates, and other internal stress fields.

The central parameters in this narrowed problem are the nature of dislocations in the matrix, the nature and distribution of the barriers

impeding glide, the resolved shear stress impelling glide, and the temperature. At zero temperature the important parameter is the critical resolved shear stress for athermal dislocation glide through the microstructure, a function of the nature and distribution of barriers.

The initial research on this problem concentrated on the motion of an isolated segment of a dislocation by cutting through or bowing around an obstacle or simple configuration of obstacles of a given type. This research continues[13] as investigators have sought more precise solutions to more realistic dislocation-obstacle models.

However, as was recognized in early research by Mott and Nabarro[20] and by Friedel,[10] the distribution of barriers is also of qualitative importance. Thus Friedel[10] argued that in high temperature glide through a random array of point barriers the nature of the activation barrier to glide would change with applied stress even though the physical nature of the obstacles remained the same. The source of the change was a statistical tendency for the dislocation to contact a greater number of obstacles per unit length as the stress increased. Mott and Nabarro[20] treated an essentially similar phenomenon in the case of diffuse barriers. This initial research led to a series of studies on the effect of the statistics of the obstacle distribution on the characteristics of dislocation glide (summarized by Kocks, Argon, and Ashby in reference 13 and by Nabarro in reference 15). This research followed the dichotomy set up by Friedel[10] and Mott and Nabarro[20] between "localized" obstacles (those whose range of significant interaction with a dislocation was small compared to their mean spacing) and "diffuse" obstacles (whose interaction fields must be considered to overlap) and reinforced their

conclusion that different theoretical techniques would be needed to handle the two cases. The "localized" obstacle approximation appears generally more applicable to hardening by small precipitates, "forest" dislocations which interact weakly in the glide plane, and dilute concentrations of solute atoms. The "diffuse" obstacle approximation appears more applicable to hardening by a higher concentration of solute atoms and by dislocations which interact strongly in the glide plane. Criteria separating the two cases have been given by Labusch.[15] To date neither case has fully yielded to theoretical attack. More theoretical progress has been made on the "localized" obstacle approximation, largely due to the observation (initially by Foreman and Makin[6]) that under suitable approximations this case could be set up for direct computer simulation.

B. Specific Problem Area

The problem of dislocation glide through a statistical distribution of localized microstructural obstacles has been the subject of extensive research from several points of view (research up to about 1972 is reviewed in reference 13). The bulk of this research addresses variants of the following basic problem (using the notation of reference 17). Consider a crystal plane which is the glide plane of a dislocation. Let it contain a random distribution of microstructural barriers, which are represented[18] as point obstacles to dislocation glide. The array is described by the statement that its points are randomly distributed and by a characteristic length

$$\ell_s = a^{1/2} \qquad \text{(I.1)}$$

where a is the mean area per point. A dislocation in this plane is modelled as a flexible, extensible string of constant line tension, Γ, and Burgers' vector of magnitude b, taken to lie in the plane. The resolved shear stress, τ, impelling glide of this dislocation may be conveniently written in dimensionless form

$$\tau^* = \tau \ell_s b/2\Gamma \qquad (I.2)$$

Let the dislocation, under the applied stress τ^*, encounter a configuration of point obstacles denoted by (i). Between two adjacent obstacles the dislocation will take the form of a circular arc of dimensionless radius R^* ($= 1/2\tau^*$). If the distance between any two adjacent obstacles along (i) exceeds $2R^*$ or if the dislocation line anywhere intersects itself, then the configuration (i) is transparent to the dislocation and will be mechanically by-passed. If (i) is not transparent, its mechanical stability is governed by the strength of the dislocation-obstacle interaction.

At the $k^{\underline{th}}$ obstacle on (i) the dislocation line forms the asymptotic angle ψ_i^k ($0 \leq \psi_i^k \leq \pi$). The force, F_i^k, that the dislocation exerts on the $k^{\underline{th}}$ obstacle is, in dimensionless form,

$$\beta_i^k = F_i^k/2\Gamma = \cos(\tfrac{1}{2}\psi_i^k) \qquad (I.3)$$

The mechanical strength of the obstacle is measured by the dimensionless parameter β_c (or angle ψ_c) and corresponds to the maximum force the obstacle can sustain without being cut or locally by-passed. A non-transparent line configuration of obstacles constitutes a mechanically stable barrier to the glide of a dislocation under stress τ^* if $\beta_i^k < \beta_c$

for all obstacles k on i, hence if $\beta_i < \beta_c$, where β_i is the maximum of the β_i^k. The smallest stress τ^* at which $\beta_i > \beta_c$ for all configurations within the array (i.e., $\beta_1 > \beta_c$, where β_1 is the minimum of the β_i) is the critical resolved shear stress, τ_c^*. When $\tau^* < \tau_c^*$ the dislocation will encounter at least one stable configuration within the array, and can glide only with the help of thermal activation.

In early work, Friedel[10] employed essentially this model to treat thermally activated glide at high temperature and low stress. He assumed that in steady state glide the pinning configuration might be approximated by a straight line of equi-spaced points with separation given by the condition that the dislocation sweep through dimensionless area one in cutting an obstacle. With these assumptions all forces (β) are the same, given by

$$\beta = (\tau^*)^{2/3} \tag{I.4}$$

and ℓ^*, the separation between adjacent obstacles, is

$$\ell^* = (\tau^*)^{-1/3} \tag{I.5}$$

Fleischer and Hibbard[5] suggested that the same model might be applied to determine the critical resolved shear stress for athermal glide through a random array of weak obstacles. Their expectation seemed confirmed by the computer simulation experiments of Foreman and Makin,[6] who determined the critical resolved shear stress for athermal glide (τ_c^*) as a function of obstacle strength (β_c) for random arrays of up to 4×10^4 points. They found good agreement with the inverse of equation (I.4) when the obstacle strength was small. Foreman and Makin

inferred that the other features of the Friedel model, e.g. equation (I.5), were also obeyed for small obstacle strengths, but apparently did not confirm this result.

In the strong obstacle limit $\beta_c \sim 1.0$, Foreman and Makin found $\tau_c^* \sim 0.82$, a result in essential agreement with the value obtained earlier by Kocks,[11] who used graphical methods. Publication of the function $\tau_c^*(\beta_c)$ by Foreman and Makin led to a series of theoretical attempts to fit it, including the "perculation" model developed by Kocks,[12] and the "unzipping" model proposed by Dorn, Guyot, and Stefansky.[3] Other pertinent theoretical work included the method of distribution functions developed by Labusch[16] (a special case of his earlier[14] estimate for the first instability in glide through an array of diffuse barriers) which yielded functional agreement with the Friedel model at low stress.

Foreman and Makin[7] and Foreman, Hirsch, and Humphries[8] continued research on glide through arrays of unlike obstacles[7] and arrays of obstacles of finite size and shape.[8] As recognized by Morris and Klahn[17] the behavior in athermal glide is strongly influenced by the characteristics of the most stable configuration encountered during glide. These most stable configurations depend on applied stress, but are identically the configurations which determine the critical resolved shear stress as a function of obstacle strength. Detailed examination of these configurations showed that while their strengths were reasonably approximated by the Friedel relation (at low stress) their other pertinent characteristics (shape, distribution of forces, distribution of segment lengths) were not. This discrepency is significant, since the distribution of

forces is important to the kinetics of low-temperature glide and since the mean segment length is a parameter often used in attempts to fit experimental data to the point obstacle model.

C. Research Problem

The continuing interest in dislocations resisted by random point barriers combined with the discrepancies between theory (the Friedel model) and the results of computer simulation provided an incentive for persuing this problem area. Two complimentary approaches were used. First, a new computer code was written enabling general and efficient simulation of the idealized problem described. Its generality enabled simulation of the present problem and is easily extendable to variants of this problem. Second, an analytic solution is derived for a limiting strength determining dislocation configuration. The strength, distribution of forces, and mean segment length defined by this solution are shown to be in good agreement with computer simulated experiments.

The generality of the analytic solution is then shown by extension to the limiting dislocation configuration in a glide plane containing a random mixture of distinct obstacles. Again, characteristics of the limiting configuration are shown to be in good agreement with computer simulation experiments. A description of the computer simulation and derivation of the limiting configurations follow.

II. COMPUTER SIMULATION

Although various computer simulations of the random array problem existed at Berkeley and elsewhere it was decided to design a new more general and efficient code. Generality enables easy modification of various sophistications. Efficiency enables sophistications and large array simulations to be reasonably computable. As simulations become more complicated and comprehensive, these attributes should prove invaluable. The new code is presently being used by E. S. P. Das at Argonne National Laboratories and has been sent to Peter Hazzledine at Oxford University. The salient features of the simulation will now be described.

Using a pseudo-random number generator the code first fills a square array of size n with a random distribution of points of density one. Each point has four parameters: 1) x location, 2) y location, 3) obstacle characteristic (e.g. the strength determining angle ψ), and 4) status parameter (denoting the obstacles status with respect to an advancing dislocation). Periodic boundaries are assumed in all directions. The code then introduces a dislocation across the lower boundary of the array and allows it to move forward until it contacts points in the array. The dislocation segments that constitute a dislocation configuration are stored in an ordered list. The list contains the following information for each segment: 1) all parameters of the obstacle on the left end of the segment, 2) the arc angle, Ω, of the bowed segment, and 3) status of the segment. Given this information the dislocation can be advanced using the algorithm now described.

The arc angle, Ω, is defined positive when the segment is bowed forward and negative when bowed backwards. Two useful properties of Ω are: 1) Ω is the tangent angle of the arc with respect to a straight line connecting the segment endpoints, and 2) the angle formed by two lines connecting any point on the arc and its end points is equal to Ω. The first property of Ω allows easy calculation of ψ, the angle made by two bowed segments adjacent to any point obstacle. The second property of Ω allows unique and easy determination of the order in which new points are encountered as a segment bows forward. Clearly the minimum Ω calculated for all points considered determines the first point the bowing segment finds. Furthermore, if the minimum Ω calculated is less than Ω_s where

$$\Omega_s = \arcsin\,[\text{segment length}/(2R)] \quad , \qquad \text{(II.1)}$$

then the segment reaches its equilibrium bow out radius, R, before any new point is encountered. The pinning points of a segment bowed to equilibrium are tested for mechanical stability by comparing the preassigned obstacle strength with resolved force exerted by the dislocation. If this occurs the segment status parameter is set to zero denoting a mechanically stable segment. Otherwise the status parameter of the segment(s) to the right of the unstable pinning point(s) is (are) set to two denoting that the obstacle to the left must be mechanically bypassed (unzipped).

Removing an obstacle from a dislocation configuration entails combining the two adjacent segments into a newly defined segment. The new segment's status parameter is set to one denoting need for advancement.

Similarly if an obstacle is encountered by an advancing segment it is incorporated into the ordered list of segments by creating two new segments replacing the old segment. Again, the new segment's status parameters are set to one.

Given a stress ($= 1/(2R^*)$), the dislocation configuration may be advanced by advancing all segments with a status parameter of one and unzipping all obstacles with a status parameter of two. When all segment status parameters are zero a mechanically stable dislocation configuration exists. Introducing a dislocation at the bottom edge of an array entails defining a dislocation consisting of straight segments (status parameters set to one) ending at equally spaced phantom points of zero strength. This dislocation will advance to the first stable configuration.

The important features of this algorithm are:

1) The dislocation is always kept intact, thus assuring all obstacles will be encountered.

2) Including more complex dislocation obstacle interactions is relatively straight forward.

3) The capability of introducing more than one dislocation exists.

4) Various non random arrays can be explored (e.g. grain boundary obstacles).

5) The stable configurations found are unique and independent of the order that unstable segments are advanced.

The algorithm described becomes much more efficient by, 1) using a two way chained list for storing the ordered dislocation segments, and

2) dividing the array of point obstacles into subarrays permitting a local search for obstacles when advancing a segment. Presently this algorithm advances a dislocation through an excess of one thousand obstacles per second on a CDC 7600 computer. Thus, the present algorithm is sufficiently general and efficient enabling more complex simulations to be explored.

Methods for determining local search regions and determining when a dislocation intersects itself are not difficult when the structure of the simulation is considered. When a stable dislocation configuration is encountered all information concerning the configuration is easily obtainable from the ordered list of dislocation segments. Given this information a method for advancing stable configurations can be chosen. One method is to increase the stress until the configuration becomes mechanically unstable. Another method is to assume a thermally activated process and to unzip accordingly. A third method is to unzip the obstacle resisting the greatest resolved dislocation force (minimum ψ). The dislocation path (set of configurations) will depend on the criteria used for advancing mechanically stable dislocations. It should be evident that characteristics of stable dislocation configurations encountered will depend on the path.

The strongest dislocation configuration at a given stress, τ^*, was determined by the minimum angle (ψ) path, i.e., given a stable configuration the dislocation was unzipped at the obstacle having the highest ratio of resolved dislocation force to preassigned obstacle strength. It can be shown that this method will find the minimum obstacle strength necessary to pin at least one dislocation. Therefore, $\beta_c(\tau_c^*)$ and

$\tau_c^*(\beta_c)$ can be uniquely determined for a given array. Furthermore, the periodic boundary conditions avoid two shortcomings of previous codes. First, prior simulations assume mirror boundary conditions which can influence dislocation configurations in a finite array. Second, the dislocation is allowed to pass through the array until the strongest configuration is encountered twice thus assuring that the entire array has been examined. The later capability will prove useful when less well defined paths are examined, e.g., thermal activation, multiple dislocations, or mobile or changing obstacles.

The code described above was used to generate the simulation data presented in the following and was also used in the simulation of the tensile deformation of an idealized crystal reported by Altintas, Hanson, and Morris (reference 1).

III. AN UPPER BOUND ON THE MOST STABLE CONFIGURATION

A. The Circle-Rolling Technique as a Branching Process

A useful device for locating the stable configurations within a random array of point obstacles is the "circle-rolling" technique described in reference 19. The dislocation line between two obstacles (say, k-1 and k) is the arc of a circle of dimensionless radius $R^* = 1/(2\tau^*)$. If k-1 and k are obstacles of strength β_c in a stable configuration at τ^* then there must be at least one obstacle (k+1) in the area swept out by rotating the circle counter-clockwise about k through an angle

$$\theta_c = \pi - \psi_c = 2 \sin^{-1} (\beta_c) \qquad \text{(III.1)}$$

Since this requirement holds for all obstacles on a stable line, the line may be generated by successive circle-rolling.

If $\tau^* < \tau_c^*(\beta_c)$ then it must be possible to locate at least one stable configuration by circle rolling. Hence, given θ_c, if there is a τ_0^* such that this technique demonstrably cannot yield a stable configuration then $\tau_0^* \geq \tau_c^*$ and is a valid upper bound. A τ_0^* is found by noting the formal similarity between the circle rolling procedure and the classical branching process in probability theory.

The classical branching process[4] contains independent events which may produce descendents of like kind, with the number of offspring given by an integer random variable of known distribution. The theory of branching processes estimates the size of the k^{th} generation descended from a single initial event. The asymptotic size of the descendent population is sharply constrained by the extinction theorem of branching

processes, which states that if $\langle n \rangle \leq 1$, where $\langle n \rangle$ is the expected number of offspring, then the line of descent will necessarily terminate after a finite number of generations.

The circle-rolling technique locates stable configurations through a type of branching process. Let the initial or zeroth segment on a configuration be that connecting an obstacle to the left hand boundary of the array. Then the first segment, if it exists, will connect the first obstacle (1) to a second (2) located in the area (A^*) swept by rotating a circle of radius R^* through an angle θ_c about (1). Each obstacle in A^* defines a possible first segment. Since A^* is a subarea of an array containing a unit density of Poisson-distributed obstacles the probability that there are exactly ν first segments (offspring) is

$$p(\nu;A^*) = \frac{(A^*)^\nu}{\nu!} e^{-A^*} \qquad \text{(III.2)}$$

The expected number of descendents in the first generation is

$$\langle n \rangle = A^* \qquad \text{(III.3)}$$

Generalizing, the k^{th} segment connects the k^{th} to the $(k+1)^{th}$ obstacle along the dislocation line. The possible k^{th} segments of a configuration are the segments which can be successfully found through sequential searches by circle rolling from the initial segment; they belong to the k^{th} generation of descent from (1). Each member of each generation has descendents whose number is governed by $p(\nu;A^*)$ with expectation A^*. A given initial segment is on a stable configuration only if it has descendents through a sufficient number of generations to reach across the array. The extinction theorem may be invoked,

and states that stable configurations cannot exist in an array of arbitrarily large size if

$$A^* \leq 1 . \qquad \text{(III.4)}$$

If the circle-rolling technique were a classical branching process the inequality (III.4) would directly yield the critical stress $(\tau_c^*(\beta_c))$ for an array of arbitrarily large size. However, the circle-rolling technique violates the assumptions of the classical branching process in two ways. First, the descendent segments found by circle-rolling are not always distinct. A particular segment may be obtainable from a given initial segment through more than one path. Second, the descendent segments are always legitimate extensions of the dislocation line. The circle-rolling may find segments which cause the dislocation line to intersect itself and hence violate a necessary number of valid dislocation segments in the k^{th} generation below the value estimated by the theory of classical branching processes. The inequality (III.4) still applies, but may be shown to yield a serious overestimate of τ_c^*. A more accurate estimate is obtained by modifying the circle-rolling procedure.

B. The Limiting Configuration Obtained Through Circle-Rolling

Let a circle of radius R^* be rotated counter-clockwise through an angle θ_c about obstacle k. The new area (A^*) swept during this operation is shown in Figure 2. The area may be described by coordinates θ and ϕ. The lines of constant θ are concave arcs generated by the leading edge of the circle as it is rotated. θ is chosen such that $0 \leq \theta \leq \theta_c$ in A^*. The lines of constant ϕ are convex arcs generated by the trailing edge

of the circle as it is rotated through an angle $\pi + \theta_c$. We choose ϕ such that $-\pi \leq \phi \leq \theta_c$ in A^*.

The advantage of this parametrization of the search area is the following. Let a point k+1 be found at (θ,ϕ) within A^* (Figure 3). Then θ is the angle of rotation between arcs k-1 and k at point k. Let t_k be a unit tangent vector to arc k-1 at point k and let $\underset{\sim}{t}_{k+1}$ be a unit tangent vector to arc k at point k+1. Then ϕ gives the angle between $\underset{\sim}{t}_k$ and $\underset{\sim}{t}_{k+1}$. Next, let a dislocation configuration (i) be generated by circle-rolling left to right then the angle at the k^{th} obstacle is θ_i^k and the direction of the line at the k^{th} obstacle is specified by the accumulated value of ϕ according to the relation

$$\underset{\sim}{t}_k = \underset{\sim}{t}_0 \exp i \left[\sum_{j=1}^{k} \phi_i^j \right] \qquad \text{(III.5)}$$

where $\underset{\sim}{t}_0$ is a unit vector perpendicular to the left-hand edge of the array and the imaginary axis is taken parallel to the left hand edge of the array.

Equation (III.5) yields an important constraint on a stable configuration. If a stable configuration is to connect the sides of an array of arbitrarily large size then it is necessary that

$$\langle \phi \rangle_i = \frac{1}{N_i} \sum_{k=1}^{N_i} \phi_i^k = 0 \quad . \qquad \text{(III.6)}$$

where N_i is the number of obstacles in the configuration. Equation (III.6) is a weak phrasing of the constraint that a stable dislocation line cannot loop onto itself. It is clearly insufficient, since $\langle \phi \rangle = 0$

on an arbitrarily long line containing a finite number of loops and also on a line containing equal numbers of loops of positive and negative sense.

Employing the constraint (III.6) along with the extinction theorem of branching processes establishes a $\tau_0^* \geq \tau_c^*(\theta_c)$ for an array of arbitrarily large size. Given an obstacle strength (θ_c) let a configuration be generated by circle-rolling left to right. Now assume a stochastic process, ignoring any illegitimacy or redundancy in descendent segments. Then in each generation the points within the search area A^* give possible extensions of the line. These points may only be used in sets which satisfy equation (III.6). Let $f(\theta,\phi)$, $0 \leq f \leq 1$, be the normalized frequency with which a point found at (θ,ϕ) is used to test the continuation of the line. We choose $f(\theta,\phi)$ to find the minimum value of R^* for which the circle rolling procedure will not necessarily fail.

Since each search area A^* is a sub-area of an array having a unit density of Poisson-distributed points, the probability that a point will be found in an element dA^* of A^* is simple dA^*. In terms of the coordinates (θ,ϕ),

$$dA^* = R^{*2} \sin(\theta - \phi)\, d\phi d\theta$$
$$= R^{*2}\, da(\theta,\phi) \qquad \text{(III.7)}$$

where $da(\theta,\phi)$ is independent of the radius. Given $f(\theta,\phi)$, the expected number of descendents in A^* is

$$n = (R^*)^2 \iint_a f(\theta,\phi)\, da(\theta,\phi) \qquad \text{(III.8)}$$

and the expected value of the coordinate ϕ is

$$\langle\phi\rangle = (R^*)^2 \iint_a \phi\, f(\theta,\phi)\, da(\theta,\phi) \ , \tag{III.9}$$

where the area $a(\theta_c)$ is the area swept when a circle of unit radius is rotated through the angle θ_c; it includes the coordinates $0 \leq \theta \leq \theta_c$, $-\pi \leq \phi \leq \theta_c$. If the circle rolling process is to be successful in an array of large size we must have $\langle n\rangle > 1$, and $\langle\phi\rangle = 0$. Incorporating these constraints and writing $R^* = 1/(2\tau^*)$, we have

$$L = \iint_a f(\theta,\phi)\, da(\theta,\phi) > 4\tau^{*2} \tag{III.10}$$

and

$$\langle\phi\rangle = \iint_a \phi\, f(\theta,\phi)\, da(\theta,\phi) = 0 \ . \tag{III.11}$$

It follows that

$$\tau_c^* < \tau_0^* = \frac{1}{2} L_0^{1/2} \tag{III.12}$$

where L_0 is the maximum value of the integral in (III.10) under the constraint (III.11).

As shown in the Appendix, L is maximized by the choice

$$f(\theta,\phi) = \begin{cases} 1 & da \in a_0(\theta_c) \\ 0 & da \in a_1 = (a - a_0) \end{cases} \tag{III.13}$$

where $a_0(\theta_c)$ (Figure 4) is the subarea of $a(\theta_c)$ over which $\phi \geq \phi_0(\theta_c)$, with $\phi_0(\theta_c)$ determined by the condition

$$\int_{-\phi_0}^{\theta_c} \phi \left[\int da(\theta,\phi)\right] = \int_{-\phi_c}^{\theta_c} \phi\, da(\phi) = 0 \ . \tag{III.14}$$

Hence a limiting configuration is formed by selecting points only from among those found in the limited subarea $R^{*2}a_0(\theta_c)$ of A^*. The limiting value of the critical stress is

$$\tau_0^* = \frac{1}{2}\left[\int_{-\phi_0}^{\theta_c} da(\phi)\right]^{1/2} \qquad \text{(III.15)}$$

The distribution of forces and segment lengths may be computed from the distribution of points within a_0.

Given the limiting function $\tau_0^*(\theta_c)$, the solution of equation (III.15), we may invert to obtain the function $\beta_0(\tau_0^*)$ where

$$\beta_0(\tau_0^*) = \sin[\tfrac{1}{2}\theta_c(\tau_0^*)] \qquad \text{(III.16)}$$

The function $\beta_0(\tau_0^*)$ places a lower bound on the obstacle strength β_c if stable configurations are to exist at stress τ_0^*. Equivalently, it sets a lower bound on the value, β_1, of the maximum force exerted on the most stable configuration encountered in glide through an array of arbitrarily large size at stress τ_0^*.

Before discussing the detailed properties of the limiting configurations we should perhaps point out that the precise configuration found by a search confined to $R^{*2}\, a_0(\theta_c)$ depends on the starting point. Since the angle ϕ measured between successive tangents left to right along a configuration differs from that measured right to left a limiting configuration generated right to left across the array will not be strictly identical to one generated left to right. Still another configuration would be formed by searching toward the two lateral boundaries of the array from an interior point. However the physical

properties of the limiting configuration (its strength, distribution of forces, and distribution of segment lengths) are uniquely independent of the starting point

C. Properties of the Limiting Configuration

To compute the properties of the limiting configuration the function $\phi_0(\theta_c)$ is required, determined by equation (III.14). The differential area

$$da(\phi) = \int^{\theta} da(\theta,\phi) \tag{III.17}$$

is

$$da(\phi) = \begin{cases} 1 - \cos(\theta_c - \phi) & 0 \le \phi \le \theta_c \\ \cos\phi - \cos(\theta_c - \phi) & \theta_c - \pi \le \phi \le 0 \\ \cos\phi + 1 & -\pi \le \phi \le \theta_c - \pi \end{cases} \tag{III.18}$$

The function $\phi_0(\theta_c)$ cannot easily be given in closed form, but is plotted in Figure 5. In the limit of small θ_c

$$\phi_0 \to k_1\theta_c \tag{III.19}$$

where

$$k_1 = \frac{1}{4}[(3 - 2\sqrt{2})^{1/3} + (3 + 2\sqrt{2})^{1/3} - 1] \tag{III.20}$$

$$\cong 0.3388 .$$

Given $\phi_0(\theta_c)$ the function $\tau_0^*(\theta_c)$ follows immediately from equations (III.15) and (III.18). The computed function $\tau_0^*(\beta_0)$ is compared to the function $\tau_c^*(\beta_c)$ obtained from computer simulation experiment in Figure 6.

The agreement between the two curves is good over the range $0 \leq \beta \leq 0.7$, which exceeds the range of obstacle strengths which recent theoretical work (Bacon, Kocks, and Scattergood[2]) suggests is physically meaningful. For $\beta > 0.7$ the theoretical curve diverges from that obtained by computer experiment, eventually approaching the limit $\tau_0^* = \sqrt{\pi/2}$ at $\beta_0 = 1.0$. This divergence is not surprising since dislocation looping becomes important at high stress, but is not properly accounted for in the derivation of equation (III.15). The problem of "overlap," or indistinguishability of descendants, may also be more serious when τ^* is large.

In the limit of small obstacle strength τ_0^* is given by the relation

$$(\tau_0^*)^2 = \frac{1}{384}\,(3x^2 + 6x + 13 + 6x^{-1} + 3x^{-2})\theta_c^3$$

$$0.7870(\theta_c/2)^3 \qquad \text{(III.21)}$$

where $x = (3 + 2\sqrt{2})^{1/3}$. This equation may be rewritten

$$(\tau_0^*) = k_2(\beta_0)^{3/2} = 0.8871(\beta_0)^{3/2} \qquad \text{(III.22)}$$

which differs from the Friedel relation (I.3) only through a multiplicative constant. Both the agreement and disagreement between equations (I.3) and (III.22) deserve comment. The agreement in functional form is not fortuitous. Virtually any technique for searching an array by rolling or bowing a circle of radius R^* through a small angle θ_c leads to a search area simple proportional to $(R^*)^2\theta_c^3$, and will hence yield an equation which differs from (I.3) only through a multiplicative constant. Regarding the disagreement, note that what we have obtained here is an upper bound on the value of τ_c^* in an array of arbitrarily large size,

which lies below the Friedel limit by ∿11%. This result may be possibly questioned on the grounds that τ_0^* also lies below the data obtained from computer simulation (Figure 6) when β is small. One should, however, recognize that the number of obstacles on the most stable configuration in a finite array is small when τ^* is small and increases with array size n only as $\sqrt{n}$. Hence the asymptotic relation obtained from computer simulation in arrays of tractable size will tend to overestimate τ_c^* for an array of infinite size.

The normalized distribution of forces along the limiting configuration may be computed from the relation

$$\rho(\theta,\tau^*)d\theta = R^{*2}\int^{\phi} da(\theta,\phi) \qquad \text{(III.23)}$$

where $\rho(\theta,\tau^*)$ is the distribution of angle θ, in the limiting configuration at stress τ_0^*. Using equation (III.7) and assigning appropriate limits to the integral we obtain

$$\rho(\theta,\tau^*) = \begin{cases} R^{*2}[1-\cos(\theta+\phi_0)] & \phi_0 \leq \pi - \theta_c \\ 2R^{*2} & \theta_c \geq \theta \geq \pi - \phi_0,\ \phi_0 \geq \pi - \theta_c \\ R^{*2}[1-\cos(\theta+\phi_0)] & \pi - \phi_0 \geq \theta \geq 0,\ \phi_0 \geq \pi - \theta_c \end{cases} \qquad \text{(III.24)}$$

For the range of interest here, $0 \leq \beta_0 \leq 0.7$, ϕ_0 is less than $(\pi - \theta_c)$ and only the first form is important. Since $\beta = \sin(\theta/2)$,

$$\rho(\beta,\tau^*) = \rho(\theta,\tau^*)d\theta/d\beta$$

$$= 2R^{*2}\{(1-\beta^2)^{-1/2}[1-(1-2\beta^2)\cos\phi_0] + 2\beta\sin\phi_0 \qquad \text{(III.25)}$$

where we have assumed $\phi_0 \leq \pi - \theta_c$. This distribution is, of course, sharply cut off at β_0. It is uniquely fixed by either τ_0^* or β_0 since either is sufficient to determine the radius R^*, the angle ϕ_0, and the maximum β_0.

The theoretical distribution (III.25) is compared to computer-generated distribution at $\tau^* = 0.1$, 0.3, and 0.5 in Figure 7. The empirical distributions were obtained by superimposing the forces found on the most stable configurations in 10 arrays of 10^4 obstacles. The fit seems good. The slight discrepancy near the cut-off value of the theoretical distribution $[\beta_0(\tau_0^*)]$ is due to the fact that the configurations found by the computer have a distribution of β_1 values near β_0.

In the limit of small obstacle strength (or, equivalently, low stress) the density of forces takes the form

$$\rho(\beta;\beta_0) \cong [(\beta/\beta_0) + k_1]^2/(k_2^2\beta_0) \qquad (\beta < \beta_0 << 1) \qquad \text{(III.26)}$$

where k_2 is defined in equation (III.22) and k_1 in equation (III.20). Note that this limiting distribution can be recast in the form

$$\rho(\beta/\beta_0) \cong [(\beta/\beta_0) + k_1]^2/k_2^2 \qquad (\beta/\beta_0 \leq 1,\ \beta_0 << 1) \qquad \text{(III.27)}$$

which is independent of τ^* or β_0. In earlier work[19] it was found that the function $\rho(\beta/\beta_1)$ might be stress-independent. While equation (III.25) suggests that this inference is not strictly correct, equation (III.27) argues that it becomes correct when τ^* is small. In fact, equation (III.25) deviates from its asymptotic form (III.27) by no more than 3% at $\tau_0^* = 0.5$. Equation (III.27) is quite accurate over the whole range of interest here.

The normalized distribution of segment lengths, $\rho(\ell^*,\tau^*)$, may be found by expressing ℓ^* as a function of θ and ϕ and finding the differential subarea of a_0 over which ℓ^* is constant. The result is, for $\phi_0 \leq \pi - \theta_c$,

$$\rho(\ell^*,\tau^*) = \begin{cases} \ell^*\theta_c & 0 \leq \ell^* \leq \ell' \\ \ell^*(\theta_c + \phi_0 - 2\sin^{-1}(\ell^*/2R^*)) & \ell' \leq \ell^* \leq \ell'' \end{cases} \tag{III.28}$$

where

$$\begin{aligned} \ell' &= 2R^* \sin(\phi_0/2) \\ \ell'' &= 2R^* \sin((\theta_c + \phi_0)/2) \end{aligned} \tag{III.29}$$

The mean segment length, $\langle \ell(\tau^*) \rangle$, is the quantity which is usually compared to the Friedel relation (I.5). Using equation (III.28),

$$\begin{aligned} \langle \ell(\tau^*) \rangle &= \int_0^{\ell''} \ell^* \rho(\ell^*,\tau^*) d\ell \\ &= (2/3)(2R^*)^3 \left\{ \cos(\phi_0/2)\left[1 - \tfrac{1}{3}\cos^2(\phi_0/2)\right] \right. \\ &\quad \left. - \cos\left(\frac{\theta_c + \phi_0}{2}\right)\left[1 - \frac{1}{3}\cos^2\left(\frac{\theta_c + \phi_0}{2}\right)\right] \right\} \end{aligned} \tag{III.30}$$

The calculated function $\langle \ell(\tau^*) \rangle$ is compared to the function $\langle \ell(\tau^*) \rangle$ obtained through computer simulation in Figure 8. The empirical curve was found by averaging the segment lengths along the most stable configuration in each of ten arrays of 10^4 obstacles at each value of τ^* for which a data bar is shown. The calculated curve closely fits the empirical data. Both curves lie below the prediction of the Friedel

model. When τ^* or θ_c is small $\langle \ell(\tau^*) \rangle$ is approximated by the asymptotic relation

$$\langle \ell(\tau^*) \rangle \sim \frac{1}{6} k_2^{-3}[(1 + k_1)^4 - k_1^4](\theta_c/2)^{-1/2}$$

$$= 0.764(\theta_c/2)^{-1/2}$$

$$= 0.734(\tau^*)^{-1/3} \qquad \text{(III.31)}$$

which suggests that the Friedel relation overestimates the asymptotic $\langle \ell(\tau^*) \rangle$, by about 33%. The two relations are, however, identical in functional form.

While the model developed here yields an excellent fit to the mean segment length $\langle \ell(\tau^*) \rangle$, it is less successful in matching the distribution of segment lengths. The density function $\rho(\ell^*, \tau^*)$ calculated from equation (III.28) is compared to that obtained from computer simulation in Figure 9. The empirical curve was determined by compiling the segment lengths found along the most stable configuration in each of 10 arrays of 10^4 points at $\tau^* = 0.1$. The calculated curve correctly predicts that $\rho(\ell^*)$ is zero when ℓ^* is significantly larger than $\langle \ell \rangle$, hence over most of the available range $0 < \ell^* < 2R^*$. However, the theoretical curve does not correctly reproduce the shape of the empirical distribution. It is not clear whether this discrepancy principally results from the approximations involved in the theoretical model or from the finite size of the arrays used to generate the empirical distribution.

IV. THE LIMITING CONFIGURATION IN AN ARRAY OF OBSTACLES OF DIFFERENT STRENGTHS

A. Extension of the Like Obstacle Limiting Configuration

When the obstacles are not identical the procedure for generating the limiting configuration must be modified slightly. Let a stable chain be constructed left to right across an array which contains randomly distributed obstacles of p distinct types, labelled $\alpha = 1,\ldots,p$, having fractions x^α and strengths β_α (or θ_α) as described in Section I. Consider the k^{th} segment of the chain, which, in the language of the branching process, is a member of the k^{th} generation of descent from the initial (or zeroth) segment. Let y_k^α be the probability that the k^{th} segment terminates at an obstacle of type α; y^α is independent of k if k is large.

If the k^{th} segment terminates at an α point then the obstacle defining the $(k+1)^{th}$ segment must be chosen from among those located in the search area of an α-obstacle, an area like that shown in Figure 2 with $\theta_c = \theta_\alpha$. This area contains an expected number of points

$$n^\alpha = (A^*)^\alpha = (R^*)^2 a^\alpha \qquad \text{(IV.1)}$$

of which an expected fraction x^β are of type β. Let $f^{\alpha\beta}(\theta,\phi)$ be the fraction of the obstacles of type β found in the differential area $da(\theta,\phi)$ which are used to extend the chain from obstacles of type α. Then the expected number of descendents (stable segments) in the $(k+1)^{th}$ generation per point in the k^{th} generation is

$$\langle n \rangle = (R^*)^2 \sum_\alpha y_k^\alpha \int_{a^\alpha} \left[\sum_\beta f^{\alpha\beta}(\theta,\phi) x^\beta \right] da(\theta,\phi) \ . \qquad \text{(IV.2)}$$

By the extinction theorem of branching processes <n> must be greater than one if the chain is to extend across an array of arbitrarily large size. The expected value of the coordinate ϕ is

$$\langle\phi\rangle = (R^*)^2 \sum_\alpha y_k^\alpha \int_{a^\alpha} \left[\sum_\beta f^{\alpha\beta}(\theta,\phi)x^\beta\right]\phi\, da(\theta,\phi) \ , \qquad \text{(IV.3)}$$

which must vanish if the chain is not to intersect itself. The expected fraction of segments of the $(k+1)^{th}$ generation which terminate at obstacles of type α is

$$y_{k+1}^\alpha = \langle n\rangle^{-1}(R^*)^2 \sum_\beta y_k^\beta \int_{a^\beta} f^{\beta\alpha}(\theta,\phi)x^\alpha da(\theta,\phi) \ . \qquad \text{(IV.4)}$$

When k is large,

$$y_{k+1}^\alpha = y_k^\alpha = y^\alpha \qquad \text{(IV.5)}$$

The limiting configuration is obtained from equations (IV.2)-(IV.5) by setting <n> = 1 and $\langle\phi\rangle = 0$, and then choosing the fractions y^α and functions $f^{\alpha\beta}(\theta,\phi)$ so that R^* is minimized (τ^* maximized) for a given set of fractions x^α and strengths θ_α. With <n> = 1 and $\langle\phi\rangle = 0$, equations (IV.2)-(IV.4) may be conveniently rewritten

$$(2\tau^*) = \int_{a^s} f(\theta,\phi)\, da(\theta,\phi) \qquad \text{(IV.6)}$$

$$0 = \int_{a^s} \phi f(\theta,\phi)\, da(\theta,\phi) \qquad \text{(IV.7)}$$

$$y^\alpha = x^\alpha\left\{\frac{1}{(2\tau^*)^2}\sum_\beta y^\beta \int_{a^\alpha} f^{\beta\alpha}(\theta,\phi)\, da(\theta,\phi)\right\} \qquad \text{(IV.8)}$$

where a^s is the search area of the obstacle of greatest strength (maximum $\theta_\alpha = \theta_s$) and where

$$f(\theta,\phi) = \sum_{\alpha,\beta} f^{\alpha\beta}(\theta,\phi)x^{\beta}y^{\alpha}h^{\alpha}(\theta) \leq \sum_{\alpha} y^{\alpha}h^{\alpha}(\theta) \tag{IV.9}$$

with

$$h^{\alpha}(\theta) = \begin{cases} 1 & 0 \leq \theta \leq \theta_{\alpha} \\ 0 & \theta > \theta_{\alpha} \end{cases} \tag{IV.10}$$

It follows directly from the theorem given in the Appendix that the integral on the right hand side of equation (IV.6) is maximized under the constraint (IV.7) if $f(\theta,\phi)$ is assigned the value

$$f(\theta,\phi) = \begin{cases} \sum_{\alpha} y^{\alpha}h^{\alpha}(\theta) & -\phi_0 \leq \phi \leq \theta_s \\ 0 & \text{otherwise} \end{cases} \tag{IV.11}$$

where ϕ_0 is the solution to the equation

$$0 = \left\{ \int_{-\phi_0}^{\theta_c} \int_{0}^{\theta_c} \phi \left\{ \sum_{\alpha} y^{\alpha}h^{\alpha}(\theta) \right\} da(\theta,\phi) \right\} . \tag{IV.12}$$

Equation (IV.8) then yields the identity

$$y^{\alpha} = x^{\alpha} \tag{IV.13}$$

and equations (IV.6) and (IV.7) may be written in the more compact form

$$(\tau_0^*)^2 = \frac{1}{4}\sum_{\alpha} x^{\alpha}a_0^{\alpha} \tag{IV.14}$$

$$0 = \sum_{\alpha} x^{\alpha}a_0^{\alpha}\langle\phi\rangle^{\alpha} \tag{IV.15}$$

where τ_0^* is the strength of the limiting configuration (an upper limit on τ_c^*), a_0^{α} is the sub-area of a^{α} over which $-\phi_0 \leq \phi \leq \theta_{\alpha}$, and $\langle\phi\rangle^{\alpha}$ is the average value of ϕ over a_0^{α}.

The sequential solution of equations (IV.15) and (IV.14) determines τ_0^*, which estimates the critical resolved shear stress, τ_c^*, for glide through an arbitrarily large array of randomly distributed obstacles having strengths θ_α ($\alpha = 1,\ldots,p$) and fractions x^α. The properties of the particular configuration which determines τ_c^* may also be approximated by the properties of the limiting configuration. Three properties are of particular interest: the fraction, c^α, of obstacles of type α in the configuration, the distribution of angles (θ) or, equivalently, of forces (β) along it, and the mean value of the separation between adjacent obstacles.

The fraction c^α is easily computed. The k^{th} generation of descent from an initial segment contains an expected fraction x^α of segments which terminate at obstacles of type α. An expected fraction $R^{*2}a_0^\alpha$ of these are continued by stable setments to points found within the optimal search area, and hence become "parents" of the $(k+1)^{th}$ generation. Since successive generations of the limiting configuration are stochastically independent, obstacles of type will appear in the limiting configuration in precisely the fraction in which they are expected as "parents" of the $(k+1)^{th}$ generation. Hence

$$c^\alpha = x^\alpha a_0^\alpha R^{*2} \qquad \text{(IV.16)}$$

The computation of the distribution of forces in the limiting configuration is also straight-forward given the discussion in section III. The fraction of obstacles of type α along the chain is given by equation (IV.16). It follows from equations (III.23)-(III.25) that, if normalization is properly accounted for, the distribution of forces on

obstacles of type α is specified by the density function

$$\rho^{\alpha}(\beta) = \begin{cases} (a_0^{\alpha} R^{*2})^{-1} \rho(\beta,\tau^*) & 0 \leq \beta \leq \beta_{\alpha} \\ 0 & \beta > \beta_{\alpha} \end{cases} \qquad \text{(IV.17)}$$

where $\rho(\beta,\tau^*)$ is the density function given by equation (III.25). The density of forces in the limiting configuration is hence

$$\rho(\beta) = \sum_{\alpha} c^{\alpha}\rho^{\alpha}(\beta) = \rho(\beta,\tau^*) \sum_{\alpha} x^{\alpha} h^{\alpha}(\beta) \qquad \text{(IV.18)}$$

where $h^{\alpha}(\beta)$ is a weighting function equal to one if $\beta \leq \beta_{\alpha}$ and to zero otherwise.

A similar argument yields the equation for the mean spacing between adjacent obstacles along the limiting configuration:

$$\langle \ell \rangle = \sum_{\alpha} x^{\alpha} \langle \ell(\tau^*) \rangle^{\alpha} , \qquad \text{(IV.19)}$$

where the function $\langle \ell(\tau^*) \rangle^{\alpha}$ is the form appropriate to (α) of the function given by equation (III.30).

$$\langle \ell(\tau^*) \rangle^{\alpha} = \left(\frac{2}{3}\right)(2R^*)^3 \left\{ \cos(\theta_{\alpha}/2)\left[1 - \frac{1}{3}\cos^2(\theta_{\alpha}/2)\right] - \cos\left(\frac{\theta_{\alpha} + \phi_0}{2}\right)\left[1 - \frac{1}{3}\cos\left(\frac{\theta_{\alpha} + \phi_0}{2}\right)\right]\right\} \qquad \text{(IV.20)}$$

B. Comparison with Computer Simulation Results

To test the accuracy of the equations developed in the previous section with computer simulation experiments consider the following. Let the obstacle (k,i) of equation (I.3) be of type α and let the mechanical strength of an obstacle of type α be β_{α}, corresponding to the

maximum force an obstacle of type α can sustain without being cut or locally bypassed. Then the dislocation is locally stable at (k,i) if

$$\beta^{*k}_i = \beta^k_i/\beta_\alpha < 1 \ . \qquad \text{(IV.21)}$$

Evaluating the quantity β^{*k}_i for each obstacle on configuration (i), with α given the value appropriate to the obstacle at (k,i), the condition for mechanical stability of (i) becomes $\beta^{*k}_i < 1$ for all k on i, hence

$$\beta^*_i < 1 \qquad \text{(IV.22)}$$

where β^*_i is the maximum of the β^{*k}_i. Next consider the following simulation experiment. If the dislocation is allowed to move through the array along a path found by passing each non-transparent configuration i at the obstacle at which β^{*k}_i (equation (IV.21)) has its maximal value (β^*_i) then the dislocation will necessarily encounter the most stable configuration within the array (this path is the analogue of the "minimal angle" path[17] through an array of like obstacles). The theory developed here approximates the strength of this configuration, in an array of large size, as $\beta^*_1 = 1.0$. The computer simulation yields an empirical value of β^*_1 for a particular array, where β^*_1 corresponds to the ratio of experimental strength with respect to the theoretical strength at a given stress, τ^*.

To compare the simulation with theory, strengths β_s and β_w were chosen with respective concentrations of x^s and x^w (= $1 - x^s$). The corresponding limiting stress τ^*_0 from equations (IV.14) and (IV.15) was computed to determine β^*_1. Three combinations of obstacle strengths were simulated at each of three choices of the fraction x^s, giving the total

of nine cases listed in Table I. For each case glide was simulated through ten arrays of 1200 obstacles. Given the finite size of these arrays, there is some scatter in the β_1^* values found and a statistical bias toward $\beta_1^* < 1.0$ which becomes more pronounced as the array size or the applied stress is decreased. Nontheless the theory appears to give a good estimate of the critical resolved shear stress τ_c^* (as measured by the agreement $\beta_1^* \sim 1.0$), the fraction c^w of weak obstacles in the configuration which determines τ_c^*, and the mean value of the interobstacle spacing along this configuration.

To test the accuracy of the force distribution predicted by equation (IV.17) an empirical force distribution for case 7 was determined by compiling the forces (β) along the most stable configurations in each of twenty-five arrays of 1200 points. The resulting normalized histogram is compared to the theoretical prediction in Figure 10. The fit seems good. It should be noted that the fit requires simultaneous estimates of the strength of the most stable configuration, the fraction of weak obstacles along it, and the distribution of forces given those parameters.

C. Extension to Thermally Activated Glide

The approach developed in Part A may also be used to estimate the velocity of thermally activated glide at low temperature. As discussed in Reference 19, when the temperature is sufficiently low the expected time required for the dislocation to transit the array, and hence the velocity of glide, is essentially determined by the expected time for the dislocation to activate past the most stable configuration it

encounters. This activation time is itself determined by the expected time for activation at the point along the most stable configuration which offers the minimum activation barrier. Defining the dimensionless time

$$t^* = \nu t \tag{IV.23}$$

where ν is the frequency with which the dislocation attempts thermal activation at an obstacle (assumed constant) and the dimensionless velocity

$$\langle v^* \rangle = n^{1/2} \langle a^* \rangle \tag{IV.24}$$

where n is the number of points in the array and $\langle a^* \rangle$ is the dimensionless area swept out per unit t^*, it follows that as T approaches zero

$$\langle v^* \rangle \simeq n^{1/2} \exp(-\Delta G_1/kT) \tag{IV.25}$$

where ΔG_1 is the minimum of the activation barriers associated with the obstacles in the most stable configuration. Computer simulation studies[19] have shown that equation (IV.25) gives a reasonable approximation to the glide velocity over a wide range of temperature.

The activation barrier ΔG at an obstacle depends[17,18] on the dislocation configuration at the obstacle (hence on β, or, equivalently on θ) and on the nature of the dislocation-obstacle interaction. If the dislocation-obstacle interaction is reasonably simple then the activation energy may be written as a function ($\Delta G(\beta)$) of the force on the obstacle. Inverting this function gives

$$\beta_\alpha = \beta_\alpha(\Delta G) \tag{IV.26}$$

or, equivalently,

$$\theta_\alpha = \theta_\alpha(\Delta G) \ , \tag{IV.27}$$

determining the force, β, or angle, θ, associated with the particular value of the activation energy for a particular type (α) of obstacle.

When conditions are such that equations (IV.25) and (IV.26) are obeyed the equations presented in Part A may be used to estimate the velocity of glide as a function of stress and temperature. Required is the function $\Delta G_1(\tau^*)$, the minimum activation energy in the most stable configuration encountered in glide at stress τ^*.

Consider an array which contains a fraction x of obstacles of type α ($\alpha = 1,\ldots,n$). Assume that equation (IV.27) is obeyed for each obstacle. Then the stress (τ^*) at which the most stable configuration encountered poses an activation barrier ΔG_1 is the maximum stress at which there exists a configuration satisfying

$$\theta_\alpha \leq \theta_\alpha(\Delta G_1) \tag{IV.28}$$

for all α. The stress $\tau^*(\Delta G_1)$ may be approximated by employing the values $\theta_\alpha(\Delta G_1)$ in place of θ_α in equations (IV.14) and (IV.15). Inverting this function gives $\Delta G_1(\tau^*)$ and consequently $\langle v^*(\tau^*,T)\rangle$ over the range of conditions for which equation (IV.25) holds.

V. DISCUSSION

The idealized model considered in this research is based on simplifying assumptions. They are: 1) constant line tension, 2) random distribution of immobile point defects, and 3) dislocation defect interaction independent of direction. The primary incentive for these assumptions is to establish a well defined general and solvable problem. Clearly these assumptions will be reasonable approximations for some real systems while failing for others. Two types of dislocation barriers, voids, and forest dislocations are now examined to illustrate this statement

First consider the constant line tension analysis. The difference between edge and screw line tension can be reasonably approximated by taking an average of their values which differ by $(1 - \nu)^{-1}$, where ν is poisson's ratio and is often between 0.2 and 0.4 for metals. Another phenomena affecting this approximation is the self interaction of two dislocation arms created at a pinning point. This effect becomes important[2] when ψ_c, the angle between the two dislocation arms, becomes small. Bacon, Kocks, and Scattergood[2] have examined this problem extensively for the case of impenetrable obstacles and have derived expressions for the effective ψ_c values for line tension analysis. They deduced, that generally, a ψ_c of less than $\pi/2$ is unstable when self interaction is included in the line tension analysis. For void defects the line tension analysis should provide a good approximation. On the other hand, forest dislocations have strain fields that can interact with the line tension. In general, any defect that has an associated strain field can affect the line tension approximation if the field of

interaction is not small relative to the defect spacing.

Next, consider the assumption of a random distribution of immobile point defects. Voids are slightly non-random due to their interaction during formation and finite size, but are generally treated as if random. However, forest dislocations tend to be non random because of their strong mutual interaction. Voids can be considered immobile while forest dislocations can be either. The point approximation for voids is reasonable since their size is small relative to their average spacing. Meanwhile forest dislocations possess a less well defined diffuse field of interaction.

Another constraint used in this model assumes that the dislocation defect interaction is independent of direction. This assumption is valid for voids. However, a gliding dislocation's interaction with a forest dislocation will be dependent on their burger vectors and can be direction dependent.

As demonstrated above, the assumptions and solution derived for the athermal critical resolved shear stress in a random array of obstacles can apply to some real dislocation systems while being unrealistic for others. To examine void defects, the real system must be non dimensionalized by equations (I.2) and (I.3). The ψ_c, obstacle strength, would have to be calculated and depends on the void size and position relative to the glide plane. Assuming that the distributions of sizes and relative glide plane positions are known, equations (IV.6) and IV.7) can be invoked to solve the characteristics of the limiting strength determining dislocation configuration. Clearly these configurations can be examined as a function of void size and density distribution. Also consider a

second defect, e.g., a strain free spherical precipitate, that reasonably adheres to the assumptions of this model. It can then be included in the analysis to determine its relative importance.

VI. CONCLUSION

As stated in the introduction, the primary goal of this research was to determine methods for examining the athermal critical resolved shear stress in a glide plane containing random point like obstacles. The two complimentary approaches of direct computer simulation and derivation of analytic expressions have proved successful. In the course of this work a useful and sufficiently general computer simulation was produced. Also, an analytic solution describing the strength, distribution of forces, and mean segment length of the strongest dislocation configuration was derived. The generality of this solution was then shown by extending it to the case of a glide plane containing a random distribution of distinct obstacles. In both cases the results were compared with computer simulation experiments and showed good agreement.

The multiple obstacle solution permits the simple treatment of cases which cannot presently be handled by computer simulation in finite time. For example consider the case of two distinct obstacle types occurring where their relative concentrations are several orders of magnitude different. To simulate a reasonable number ($\sim 10^3$) of dilute obstacles could require an array of unmanageable size. Alternately, the simulation code should prove useful for examining more complete and complicated dislocation models.

ACKNOWLEDGEMENTS

This work was done under the auspices of the United States Energy Research and Development Administration.

My sincere thanks to Bill Morris for providing guidance and constant encouragement, and to Jack Washburn and Frank Hauser for reviewing this manuscript, and to Madeleine Penton for typing and retyping this manuscript.

I would like to acknowledge the staff and faculty in both the Hearst Mining Building and Building 62, especially Shirley Ashley and Doug Kreitz.

Many thanks to Sabri Altintas for useful discussions, and to Norris Hagan for programming assistance.

Thanks is due to my parents and sister, Marilyn, for their constant encouragement and support.

My love and warm gratitude to my wife, Janie, whose love has provided direction and purpose in my life and work.

APPENDIX

Choose $f(\theta,\phi)$ such that the integral

$$L = \iint_a f(\theta,\phi)\,da(\theta,\phi) \tag{A.1}$$

is maximized subject to the constraints

$$f(\theta,\phi) \leq 1 \tag{A.2}$$

$$\iint_a \phi f(\theta,\phi)\,da(\theta,\phi) = 0 \tag{A.3}$$

where a is the search area of Figure 2, defined by $0 \leq \theta \leq \theta_c$, $-\pi \leq \phi \leq \theta_c$. The solution is

$$f(\theta,\phi) = \begin{cases} 1 & da \in a_0 \\ 0 & da \in a_1 = (a - a_0) \end{cases} \tag{A.4}$$

where a_0 is the subarea defined by $0 \leq \theta \leq \theta_c$, $-\phi_0 \leq \phi \leq \theta_c$, with ϕ_0 determined by the condition

$$\int_{-\phi_0}^{\theta_c} \phi\left[\int_0^{\theta_c} da(\theta,\phi)\right] = \int_{-\phi_0}^{\theta_c} \phi\,da(\phi) = 0 \tag{A.5}$$

The proof is straightforward. Let $q(\theta,\phi)$ be a piece-wise continuous function, $0 \leq q \leq 1$ such that

$$f(\theta,\phi) = \begin{cases} 1 - q(\theta,\phi) & da \in a_0 \\ q(\theta,\phi) & da \in a_1 \end{cases} \tag{A.6}$$

and define

$$L_0 = \iint_{a_0} da(\theta,\phi). \tag{A.7}$$

Then

$$L - L_0 = \Delta L = J_1 - J_0 \tag{A.8}$$

where

$$J_i = \iint_{a_i} q \, da \geq 0 \tag{A.9}$$

From equations (A.3) and (A.5)

$$K_1 = K_0 \, , \tag{A.10}$$

$$K_i = \iint_{a_i} (-\phi) q \, da \, . \tag{A.11}$$

It follows from the mean value theorem and the condition $\phi_0 \leq (-\phi) \leq \pi$ in a_1, that

$$K_1 = (\phi_0 + N) J_1 \tag{A.12}$$

where $N \geq 0$. Similarly,

$$K_0 = (\phi_0 - M) J_0 \tag{A.13}$$

where $M \geq 0$. Equations (A.10) and (A.9) then require that $M \leq \phi_0$ and

$$J_1 = \left[\frac{\phi_0 - M}{\phi_0 + N} \right] J_0 \leq J_0 \tag{A.14}$$

Hence $\Delta L \leq 0$ for arbitrary $q(\theta,\phi)$. The equality holds only if $q = 0$, which establishes equation (A.4).

REFERENCES

1. S. Altintas, K. Hanson, and J. W. Morris, Jr., J. Materials and Technology (in press).

2. D. J. Bacon, U. F. Kocks, and R. O. Scattergood, Phil. Mag. 28, 1241 (1973).

3. J. E. Dorn, P. Guyot and T. Stefansky, Physics of Strength and Plasticity, A. S. Argon, ed. (MIT, Cambridge, 1969), p. 133.

4. W. Feller, An Introduction to Probability Theory and its Applications, 2nd ed. (Wiley, New York, 1957), Vol. I.

5. P. L. Fleischer and W. R. Hibbard, in The Relation Between the Structure and Mechanical Properties of Metals (H. M. Stationary Office, London, 1963), p. 262.

6. A. J. E. Foreman and M. J. Makin, Phil. Mag. 14, 911 (1966).

7. A. J. E. Foreman and M. J. Makin, Can. J. Phys. 45, 571 (1967).

8. A. J. E. Foreman, P. B. Hirsch, and F. J. Humphries, Fundamental Aspects of Dislocation Theory (NBS Pub. #317, 1970), Vol. 2, p. 1083.

9. J. Friedel, in Electron Microscopy and Strengths of Crystals, G. Thomas and J. Washburn, eds. (J. Wiley, New York, 1963), p. 605.

10. J. Friedel, Dislocations (Addison-Wesley, Reading, Mass., 1964), p. 229.

11. U. F. Kocks, Phil. Mag. 13, 541 (1966).

12. U. F. Kocks, Can. J. Phys. 45, 737 (1967).

13. U. F. Kocks, A. S. Argon, and M. F. Ashby , "Thermodynamics and Kinetics of Slip," Argonne National Laboratory, Material Science Division, Technical Report, August 1973.

14. R. Labusch, Phys. Stat. Solidi 41, 659 (1970).

15. R. Labusch, Acta Met. 20, 917 (1972).

16. R. Labusch, ref. 15; also in J. C. M. Li, ed., Rate Phenomena in Plastic Deformation (Plenum Press, in press).

17. J. W. Morris, Jr. and Dale H. Klahn, J. Appl. Phys. 44, 4882 (1973).

18. J. W. Morris, Jr. and C. K. Syn, J. Appl. Phys. 45, 961 (1974).

19. J. W. Morris, Jr., and Dale H. Klahn, J. Appl. Phys. 45, 2027 (1974).

20. Summarized by F. R. N. Nabarro, J. Less Common Metals 28, 257 (1972).

21. S. I. Zaitsev and E. M. Nadgonyi , Sov. Phys. Solid State 15, 1777 (1974).

Table I. A comparison of the predicted values of β_1^* (= 1.0), c^w, and $\langle \ell \rangle$ with the mean of the values found through computer simulation for the most stable configuration in each of ten arrays of 1200 points under each of the nine conditions shown.

Case	β_s	β_w	x^w	τ_0^*	$\langle \beta^* \rangle_{exp}$	c^w_{theory}	$\langle c^w \rangle_{exp}$	ℓ_{theory}	$\langle \ell \rangle_{exp}$
1	0.5	0.2	0.5	0.240	1.006	0.13	0.13	1.30	1.28
2	0.5	0.05	0.5	0.231	0.998	0.020	0.021	1.44	1.46
3	0.2	0.05	0.5	0.057	0.919	0.064	0.071	2.25	2.08
4	0.5	0.2	0.17	0.299	0.997	0.030	0.041	1.11	1.05
5	0.5	0.05	0.17	0.297	1.002	0.0042	0.0048	1.13	1.12
6	0.2	0.05	0.17	0.073	0.948	0.014	0.015	1.84	1.73
7	0.5	0.2	0.83	0.157	0.969	0.40	0.44	1.65	1.59
8	0.5	0.05	0.83	0.135	1.007	0.088	0.145	2.31	2.26
9	0.2	0.05	0.83	0.035	0.890	0.24	0.23	3.21	3.01

FIGURE CAPTIONS

Figure 1. Detail of mechanical equilibrium in the i^{th} obstacle configuration.

Figure 2. Parametrization of the area searched by circle-rolling to an angle $\theta_c = \pi$.

Figure 3. Diagram illustrating that the angle ϕ_k measures the change in direction of the dislocation line at obstacle (k+1).

Figure 4. Division of the search area (a) into the limiting area (a_0) and the excess area (a_1) by the coordinate line $\phi = -\phi_0$.

Figure 5. The limiting parameter $\phi_0(\theta_c)$.

Figure 6. The limiting stress $\tau_0(\beta_0)$ compared to the function $\tau^*(\beta_1)$ obtained by direct computer simulation of glide through arrays of 10^4 obstacles. The bars include the values of the maximum force (β_1) in the most stable configuration encountered in glide through each of ten arrays of 10^4 points at each value of the stress τ^* for which a data bar is shown.

Figure 7. The distribution of forces in the limiting configuration compared to histograms obtained through direct computer simulation of glide through arrays of 10^4 points. The limiting forces (β_0) are: $\beta_0 = 0.2322$ at $\tau^* = 0.1$, $\beta_0 = 0.4751$ at $\tau^* = 0.3$, $\beta_0 = 0.6526$ at $\tau^* = 0.5$.

Figure 8. The mean segment length $\langle \ell(\tau^*) \rangle$ in the limiting configuration compared to that predicted by the Friedel relation (equation I.5) and that determined by direct computer simulation of glide through arrays of 10^4 points. The data bars include the mean segment length in the most stable configuration in each of ten arrays of 10^4 points at each value of the stress for which a data bar is shown.

Figure 9. The distribution of segment lengths in the limiting configuretion at $\tau^* = 0.1$ compared to a histogram determined by direct computer simulation of dislocation glide through arrays of 10^4 points at $\tau^* = 0.1$. The mean segment length $\langle \ell^* \rangle$ is 1.572 in the limiting distribution compared to 1.493 for the histogram.

Figure 10. The theoretical distribution of forces (β) in the limiting configuration for case number 7 (Table I) compared to an empirical histogram obtained through computer simulation as described in the text.

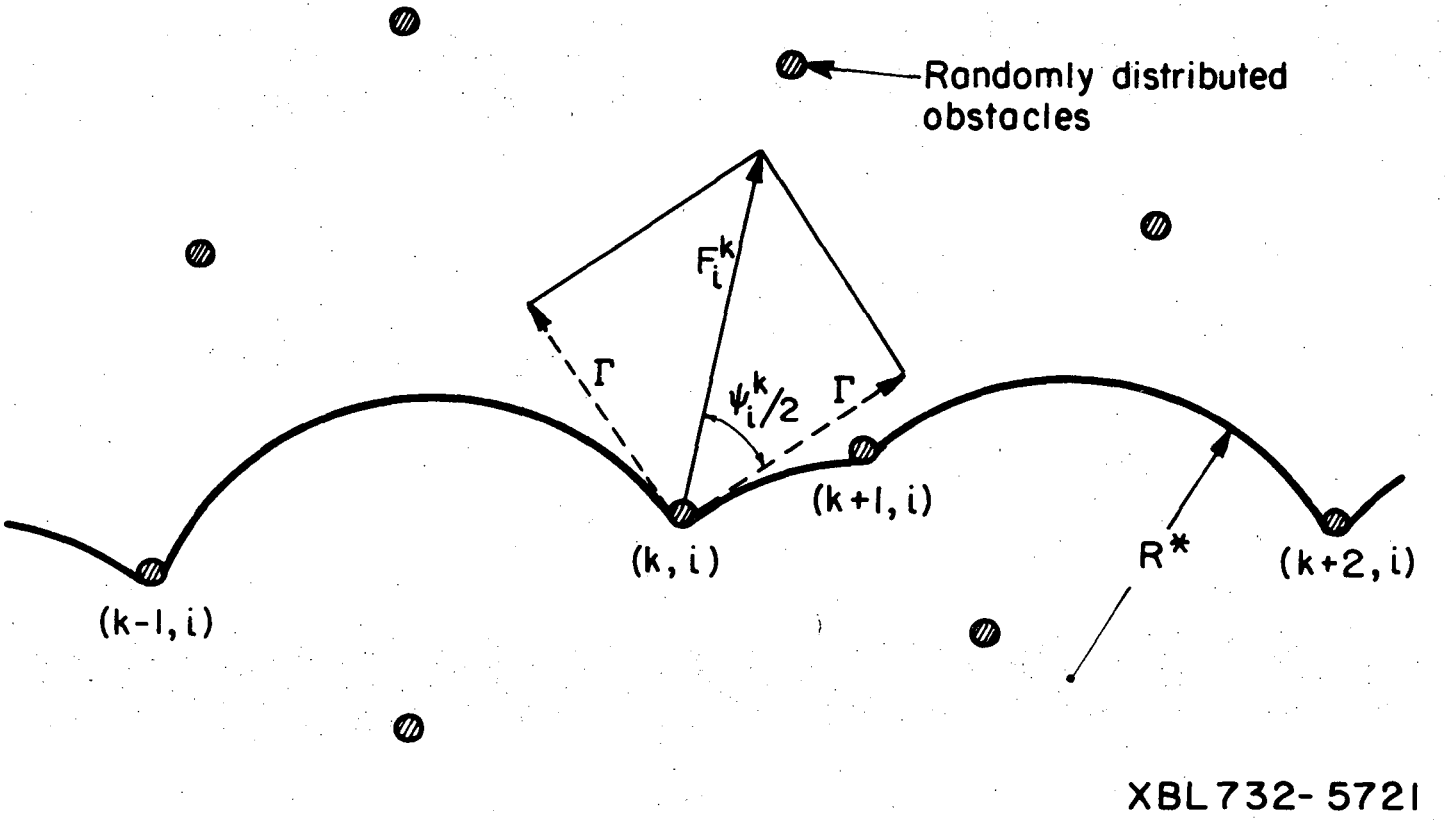
Randomly distributed obstacles
F_i^k
Γ
$\psi_i^k/2$
Γ
(k-1, i)
(k, i)
(k+1, i)
R*
(k+2, i)
XBL732-5721

Figure 1

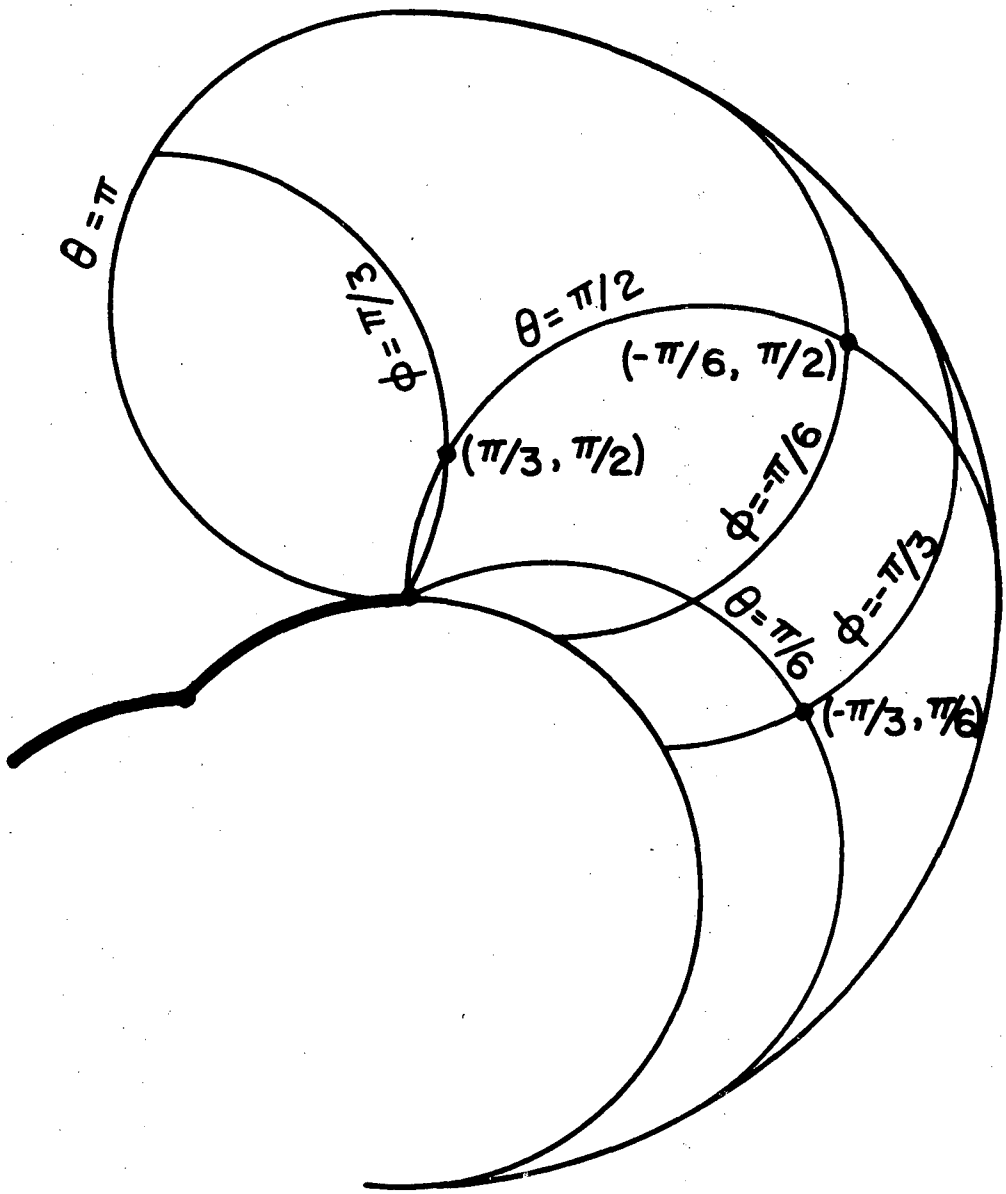

XBL748-6938

Figure 2

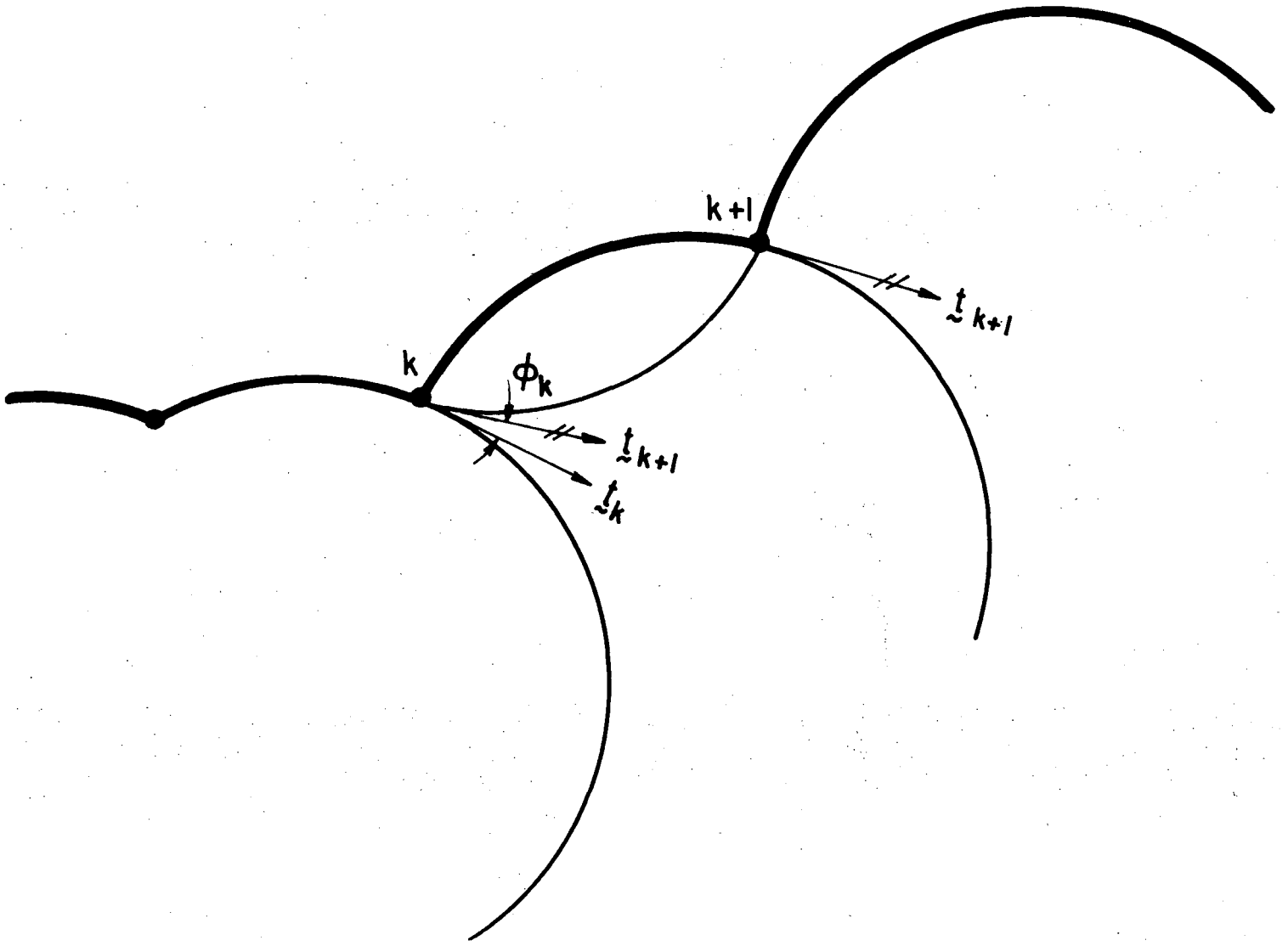

XBL748-6939

Figure 3

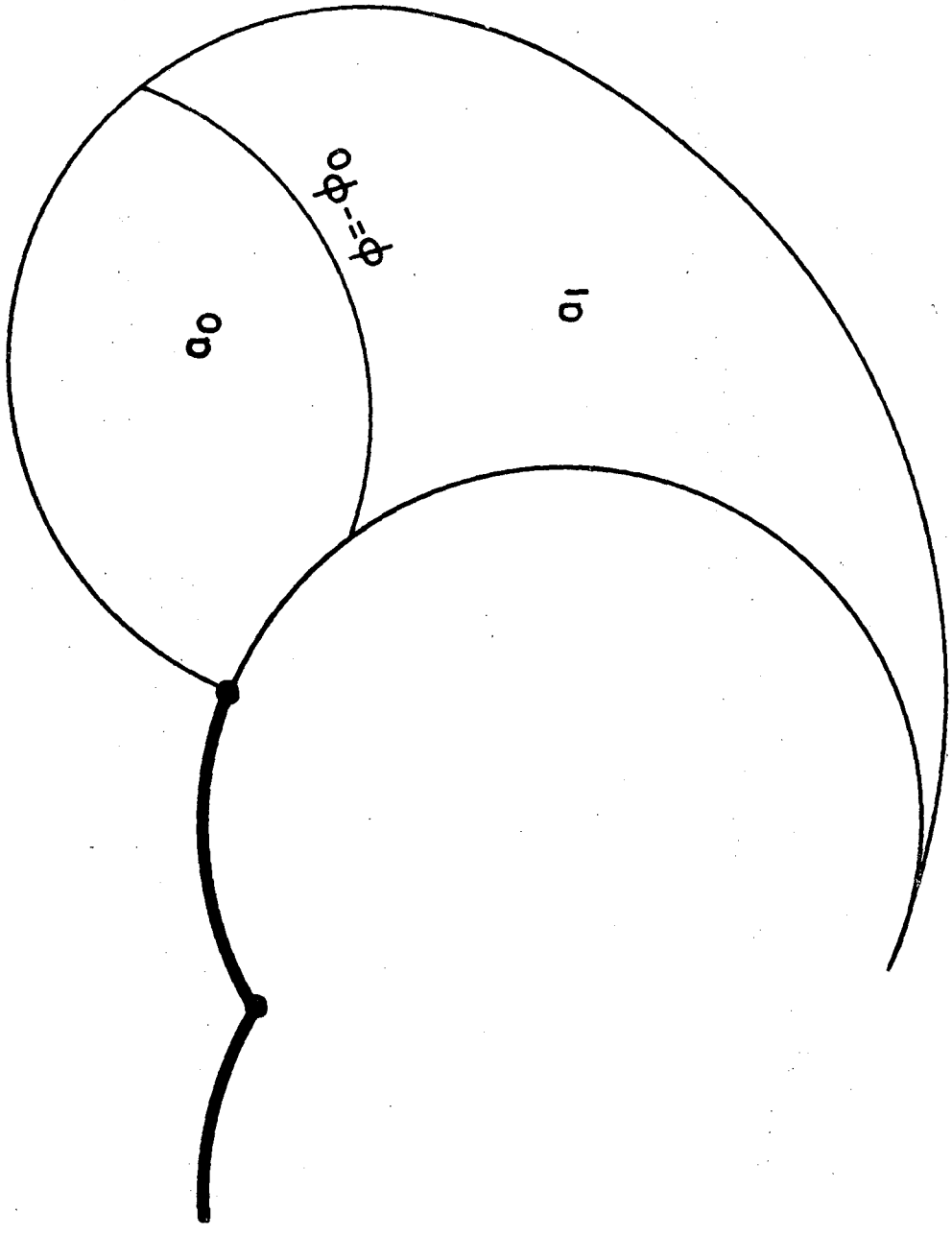

XBL 748-6940

Figure 4

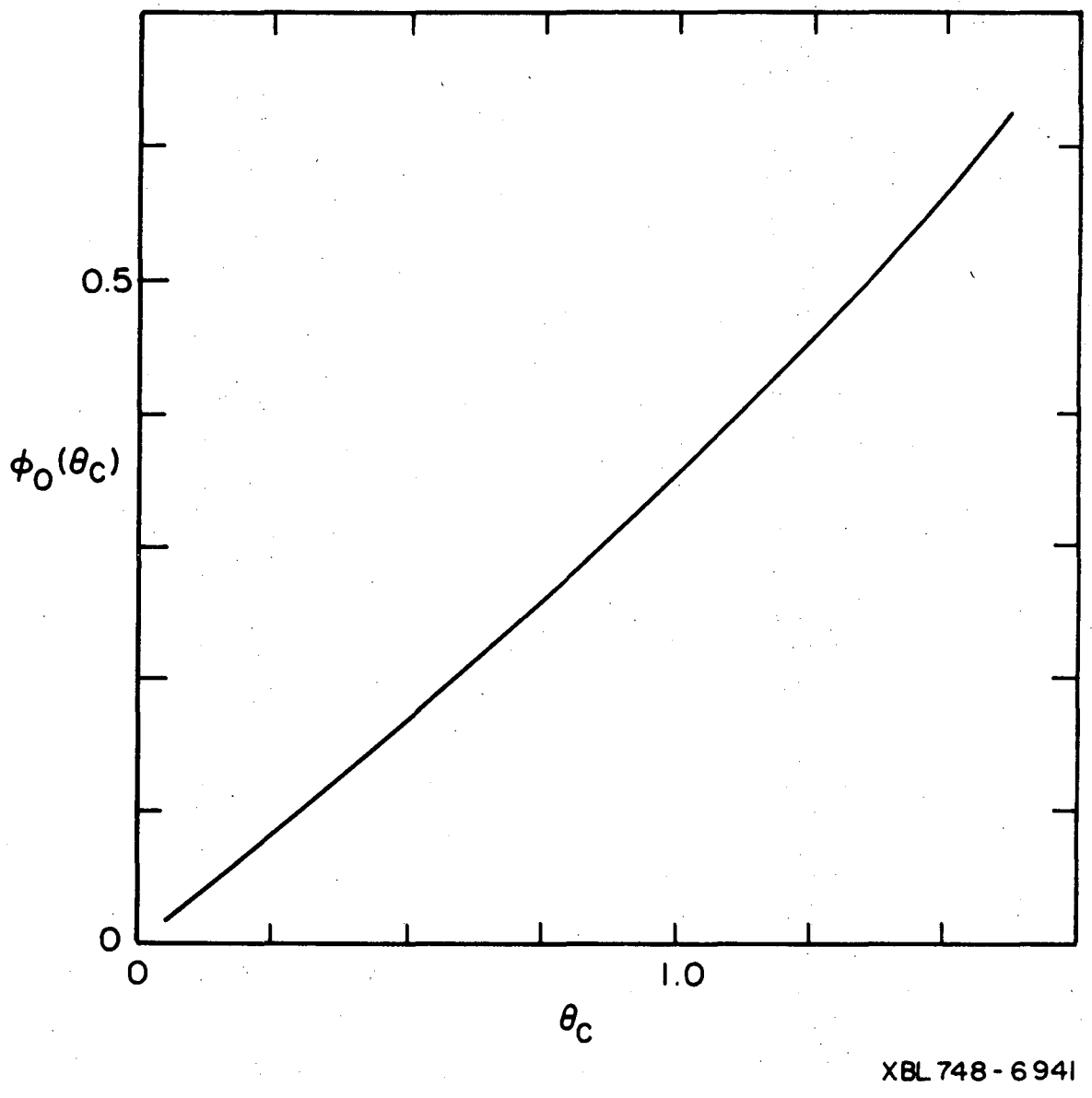

Figure 5

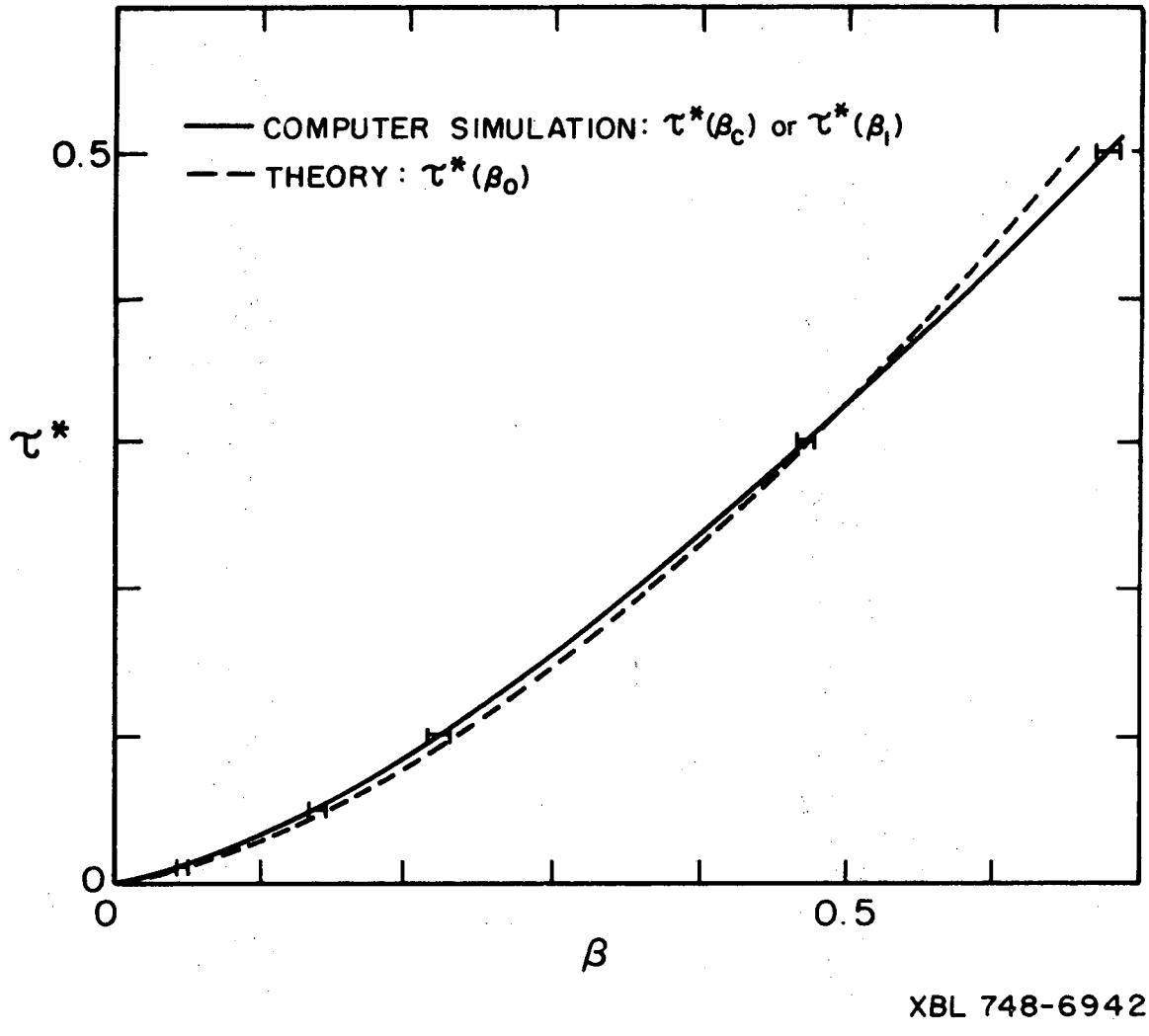

Figure 6

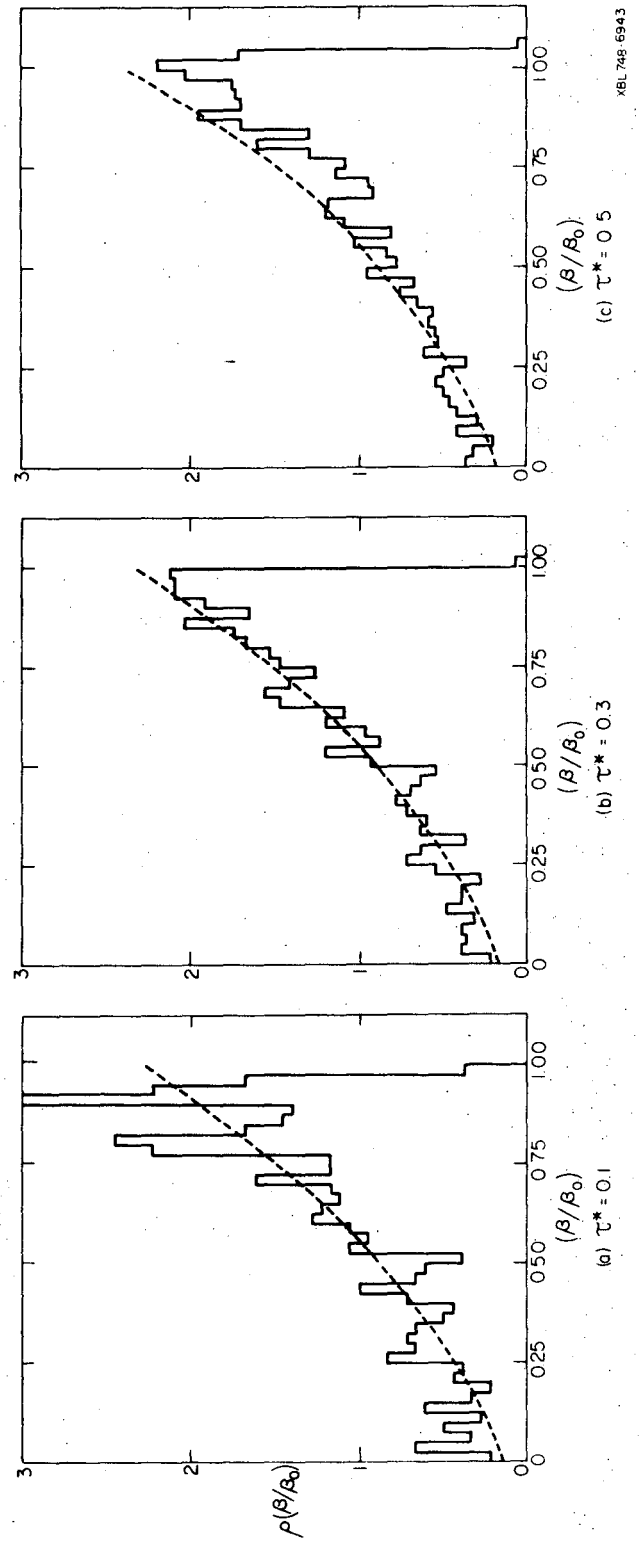
$\rho(\beta/\beta_0)$
0
1
2
3
0
0.25
0.50
0.75
1.00
(β/β_0)
(a) $\tau^* = 0.1$
(b) $\tau^* = 0.3$
(c) $\tau^* = 0.5$
XBL 748-6943

Figure 7

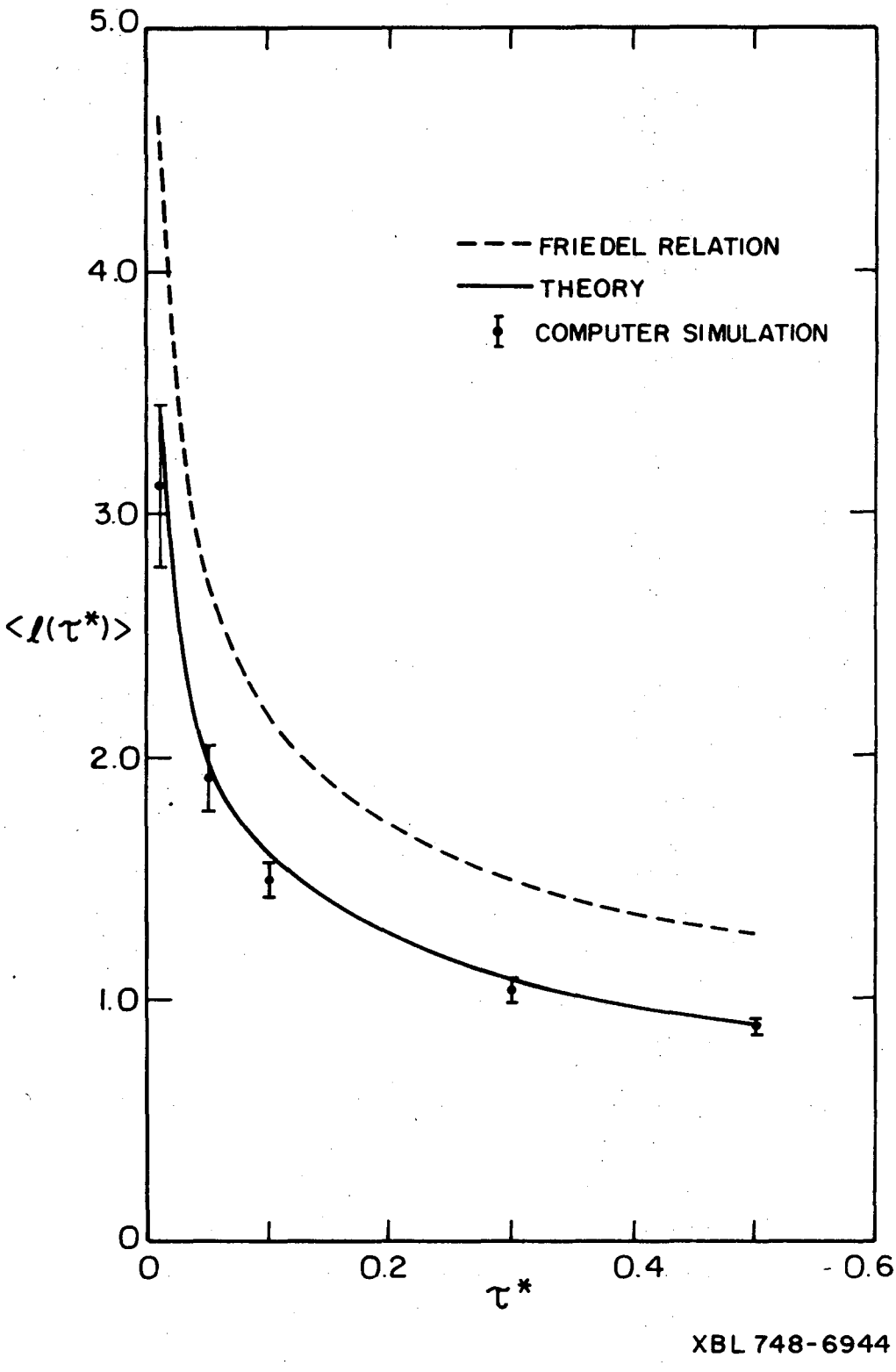

Figure 8

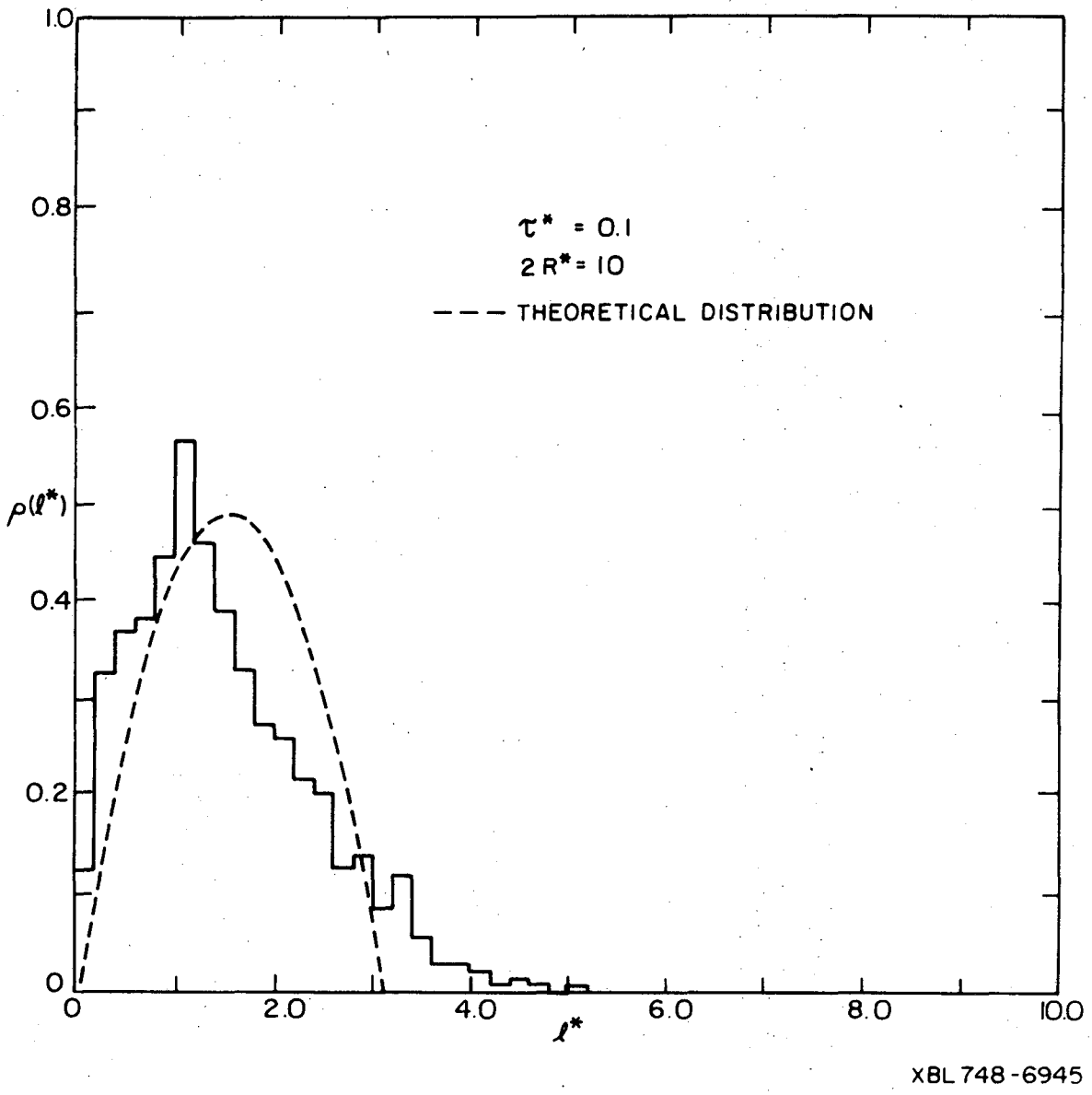
1.0
0.8
0.6
0.4
0.2
0
$\rho(\ell^*)$
$\tau^* = 0.1$
$2R^* = 10$
THEORETICAL DISTRIBUTION
0
2.0
4.0
6.0
8.0
10.0
ℓ^*
XBL 748-6945

Figure 9

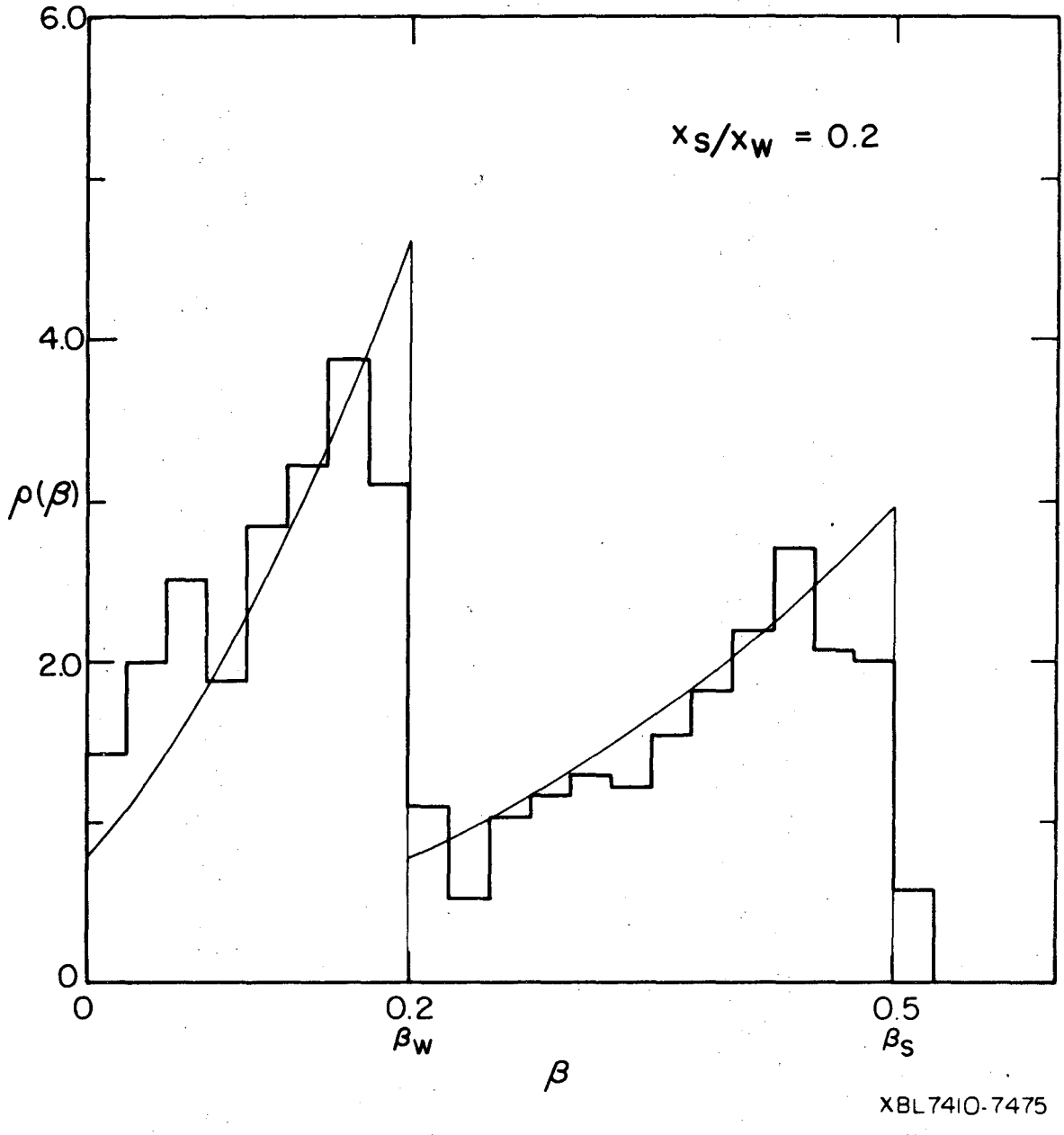

Figure 10

TECHNICAL INFORMATION DIVISION
LAWRENCE BERKELEY LABORATORY
UNIVERSITY OF CALIFORNIA
BERKELEY, CALIFORNIA 94720